Author Manuscript

Author Manuscript

Author Manuscript

Author Manuscript

HHS Public Access

Author manuscript

Immunity. Author manuscript; available in PMC 2017 April 19.

Published in final edited form as:

Immunity. 2016 April 19; 44(4): 924–938. doi:10.1016/j.immuni.2016.03.012.

Expansion and activation of CD103+ dendritic cell progenitors at the tumor site enhances tumor responses to therapeutic PD-L1 and BRAF inhibition

Hélène Salmon[1,2,3], **Juliana Idoyaga**[5], **Adeeb Rahman**[4], **Marylène Leboeuf**[1,2,3], **Romain Remark**[2,3], **Stefan Jordan**[1,2,3], **Maria Casanova-Acebes**[1,2,3], **Makhzuna Khudoynazarova**[1,2,3], **Judith Agudo**[2,3,4], **Navpreet Tung**[1,2,3], **Svetoslav Chakarov**[9], **Christina Rivera**[1,2,3], **Brandon Hogstad**[1,2,3], **Marcus Bosenberg**[6], **Daigo Hashimoto**[7], **Sacha Gnjatic**[2,3], **Nina Bhardwaj**[2,3], **Anna Karolina Palucka**[8], **Brian D. Brown**[2,3,4], **Joshua Brody**[2,3], **Florent Ginhoux**[9], and **Miriam Merad**[1,2,3]

[1]Department of Oncological Sciences, Icahn School of Medicine at Mount Sinai, New York, NY, USA

[2]Tisch Cancer Institute, Icahn School of Medicine at Mount Sinai, New York, NY, USA

[3]Immunology Institute, Icahn School of Medicine at Mount Sinai, New York, NY, USA

[4]Department of Genetics and Genomic Sciences, Icahn School of Medicine at Mount Sinai, New York, NY, USA

[5]Department of Microbiology and Immunology, Stanford University School of Medicine, Stanford, CA, USA

[6]Yale University School of Medicine, New Haven, CT, USA

[7]Department of Hematology, Hokkaido University Graduate School of Medicine, Sapporo, Japan

[8]The Jackson Laboratory for Genomic Medicine, Farmington, CT, USA

[9]Singapore Immunology Network, Agency for Science, Technology and Research, Biopolis, Singapore.

Abstract

Corresponding Author: Miriam Merad, miriam.merad@mssm.edu.

Publisher's Disclaimer: This is a PDF file of an unedited manuscript that has been accepted for publication. As a service to our customers we are providing this early version of the manuscript. The manuscript will undergo copyediting, typesetting, and review of the resulting proof before it is published in its final citable form. Please note that during the production process errors may be discovered which could affect the content, and all legal disclaimers that apply to the journal pertain.

AUTHOR CONTRIBUTIONS

H.S. and J.I. conceived and performed experiments, and wrote the manuscript. A.D., M.L., R.R., M.C-A., M.K, J.A., C.R., B.H., N.T. and S.C. performed experiments. D.H., S.G., N.B., A.K.P., B.B., J.B. and F.G. provided expertise and feedback. M.B. and J.B. provided reagents. A.K.P. provided funding. M.M. conceived experiments, wrote the manuscript and provided funding.

eTOC Blurb

Large numbers of melanoma patients develop resistance to targeted therapy or fail to respond to checkpoint inhibition. Merad and colleagues show that expansion and activation CD103^{+} DC progenitors at the tumor site enhance tumor responses to BRAF and PD-L1 blockade.

Author Manuscript Author Manuscript Author Manuscript Author Manuscript

Large numbers of melanoma lesions develop resistance to targeted inhibition of mutant BRAF or fail to respond to checkpoint blockade. We explored whether modulation of intratumoral antigen presenting cells (APCs) could increase responses to these therapies. Using mouse melanoma models, we found that $CD103^+$ dendritic cells (DCs) were the only APCs transporting intact antigens to the lymph nodes and priming tumor-specific $CD8^+$ T cells. $CD103^+$ DCs were required to promote anti-tumoral effects upon blockade of the checkpoint ligand PDL1; however, PD-L1 inhibition only led to partial responses. Systemic administration of the cytokine Flt3L followed by intratumoral poly I:C injections expanded and activated $CD103^+$ DC progenitors in the tumor, enhancing responses to BRAF and PD-L1 blockade and protecting mice from tumor rechallenge. Thus, the paucity of activated $CD103^+$ DCs in tumors limits checkpoint blockade efficacy and Flt3L-poly I:C therapy can enhance tumor responses to checkpoint and BRAF blockade.

Graphical Abstract

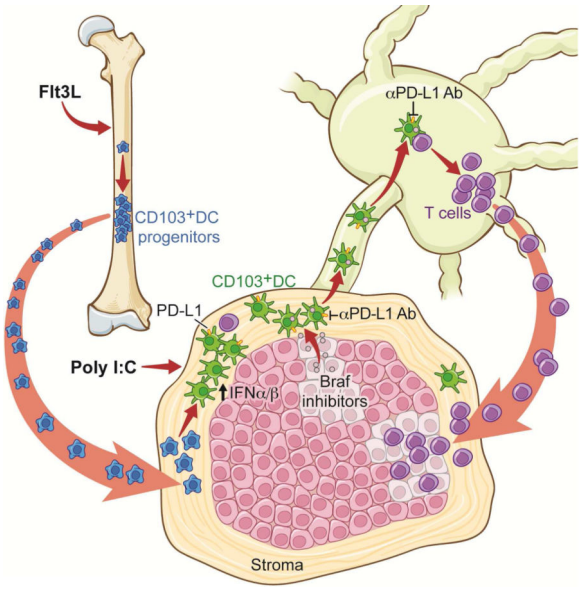

INTRODUCTION

Two classes of drugs, inhibitors of BRAF signaling (Flaherty et al., 2010) and checkpoint inhibitors (Sharma and Allison, 2015a, b) have recently achieved substantial survival advantages in melanoma patients. Despite initial high clinical responses to BRAF blockade in $BRAF^{V600E}$-mutated melanoma patients, most tumor lesions relapse within few months after therapy initiation (Flaherty et al., 2010). BRAF inhibition can induce tumor cell death and the release of tumor antigens, and therefore represents a unique opportunity to increase T cell immunity against readily available tumor-associated antigens (Kroemer et al., 2013).

Three checkpoint inhibitors have been actively explored clinically including Abs to cytotoxic lymphocyte antigen 4 (CTLA-4), programmed cell death 1 (PD-1) and to the checkpoint ligand PD-L1 (Page et al., 2014). PD-L1 is expressed mostly on steady state APCs and can be upregulated upon exposure to inflammatory signals (Keir et al., 2008), on APCs and tumor cells. Upon TCR engagement with cognate antigens, PD-L1 binds to PD-1

Author Manuscript Author Manuscript Author Manuscript Author Manuscript

on T cells and modulates T cell activation by inducing TCR stop signals (Fife et al., 2009; Yokosuka et al., 2012).

Despite significant clinical benefits, high numbers of cancer patients fail to respond to checkpoint blockade. Prior studies suggest that checkpoint inhibition may not be sufficient in patients that have limited tumor immune cell infiltration (Fuertes et al., 2011; Gajewski et al., 2013; Herbst et al., 2014; Sharma and Allison, 2015a). However, while T cells are found accumulating in the tissue stroma surrounding the tumor mass in most human tumors, they are rarely found interacting with tumor cells (Galon et al., 2006; Salmon et al., 2012). In a fraction of patients that resist anti-PD-L1 mAb therapy, $CD8^+$ T cells localize at the edge of the tumors whereas they accumulate in the tumor mass in patients that respond to PD-L1 blockade, (Herbst et al., 2014; Tumeh et al., 2014) suggesting that in addition to PD-L1 inhibition, strategies aiming at promoting T cell accumulation in the tumor mass are essential for the induction of therapeutic immunity.

Through their ability to produce T cell-specific chemokines and present antigens together with costimulatory or inhibitory signals, tumor-associated APCs are best poised to shape anti-tumoral effector immunity. Most inflamed tissues harbor heterogeneous populations of APCs that comprise DCs, macrophages, monocytes and monocyte-derived cells (Merad et al., 2013). Tissue-resident DCs consist of two functionally specialized subsets: the $CD103^+$-$CD8^+$ DCs that excel in the priming and cross-presentation of cell-associated antigens to $CD8^+$ T cells and $CD11b^+$ DCs that are more potent at driving $CD4^+$ helper T cell responses (Merad et al., 2013). Analogous counterparts to these populations have been identified in humans and include $CD141^+$ and $CD1c^+$ DCs, respectively (Guilliams et al., 2014). Previous results suggest that melanoma lesions enriched in type I interferon (IFN)-induced genes are also rich in T cells and that type I IFN production by the $CD103^+$-$CD8^+$ DC lineage controls spontaneous T cell priming to tumor antigens (Fuertes et al., 2011). Thus, the composition of the tumor-associated myeloid compartment likely plays a key role in tumor response to checkpoint blockade.

In this study, we examined the composition of tumor-associated myeloid cells of two different melanoma lesions at different time points during tumor growth. We probed their contribution to the transport of tumor antigens to the tumor-draining LN (TdLN), induction of anti-tumoral effector T cells and to shaping clinical response to checkpoint inhibition. Our results revealed that increased myeloid cell commitment to the $CD103^+$ DC lineage and activation of intratumoral $CD103^+$ DCs could substantially enhance the clinical response to checkpoint and BRAF blockade.

RESULTS

$CD103^+$ and $CD11b^+$ DCs represent minor cell populations infiltrating *Braf-mutant* and B16 melanoma lesions

To characterize the diversity of tumor-associated myeloid cells, we used two experimental models of melanoma tumors: B16 tumor graft and the Tyr::CreER;$Braf^{CA}$/$Pten^{loxP}$/$Ctnnb1^{loxex3}$ tumor model in which the $Braf^{V600E}$ mutation, Pten deletion and a mutated form of β-catenin that increases its stability are enforced in melanocytes upon cutaneous

Author Manuscript Author Manuscript Author Manuscript Author Manuscript

application of 4-hydroxytamoxifen (4-HT), leading to the formation of advanced melanoma lesions within 3 weeks (Damsky et al., 2011).

In both tumor lesions, myeloid cells accounted for more than 60% of $CD45^+$ cells and consisted mostly of monocytes and macrophages. DCs represented only a minor cell population reaching no more than 5% of myeloid cells (Figure 1A). To more thoroughly evaluate the tumor-infiltrating immune populations, we used Time of Flight mass cytometry (CyTOF) and analyzed B16 tumors at two different time points. SPADE analysis revealed an accumulation of monocytes that paralleled a reduced DC/monocyte-derived cell ratio over time (Figure 1B). Similar data were obtained using flow cytometry (Figure S1B). Both $CD103^+$ and $CD11b^+$ DC subsets were present in tumor lesions, although in very low numbers, along with macrophages and $Ly6C^{hi}MHCII^{hi}$ cells, referred to as "monocyte-derived cells". Monocyte-derived cells and macrophages expressed the monocyte markers CCR2 and CD115, the macrophage markers MertK, F4/80 and CD64, as well as detectable levels of CD11c (Figure S1C).

To characterize DC and macrophage localization in the tumor mass, we generated fluorescent-reporter inducible melanoma lesions by crossing C57BL/6 Tyr::CreER;$Braf^{CA}$/$Pten^{loxP}$ mice with Tomato reporter mice. We also used B16-YFP tumor cell lines where melanoma cells are positive for the yellow fluorescent protein (YFP). Whereas macrophages and monocyte-derived cells were distributed throughout the tumor, DCs were sparsely distributed and rarely infiltrated the tumor mass (Figure 1C). Consistent with these findings, human melanoma lesions were poorly infiltrated by DCs, in particular $CD1c^+$ and $CD141^+$ DCs, compared to $CD68^+$ macrophages which accumulated throughout the tumor (Figure 1D and Figure S1D). These results emphasize the paucity of tumor-infiltrating DCs in mouse and human melanoma lesions.

$CD103^+$ DC is the only intratumoral myeloid cell population that transports intact antigens to the tumor-draining lymph nodes

We tracked the capture of tumor-associated fluorescent antigens by each myeloid cell compartment using confocal microscopy and flow cytometry (Figures 1E-1H). Macrophages were by far the most potent cells at capturing tumor-associated fluorescence (Figures 1E and S1E) which accumulated as puncta in intracellular compartments consistent with antigen phagocytosis (Figure S1F). Although most myeloid cells captured tumor-associated fluorescence at the tumor site, $CD103^+$ DCs were the only myeloid cells carrying intact tomato-or YFP-fluorescent proteins to the TdLN, in both models (Figures 1F and 1G). YFP^+ $CD103^+$ DCs were strongly reduced in the TdLN of mice lacking Ccr7, a chemokine receptor required for DC migration to the LN (Forster et al., 1999), compared to $Ccr7^{+/+}$ mice, suggesting that tumor-associated fluorescence was actively transported by tissue migratory $CD103^+$ DCs to the LN (Figure 1H). $CD11b^+$ migratory DCs, LN $CD64^+$ macrophages and monocyte-derived cells were negative for tomato and YFP (data not shown), suggesting that they either failed to transport tumor-associated antigens or efficiently degraded the fluorescence in the TdLN. To address this question, mice were injected with B16 tumors expressing the model antigen ovalbumin (B16-OVA) and migratory and LN-resident DCs were isolated from the TdLN by fluorescence activated cell

Author Manuscript Author Manuscript Author Manuscript Author Manuscript

sorting (FACS) and co-cultured with OVA-specific TCR transgenic OT-I $CD8^+$ T cells labeled with the cell proliferation dye, CFSE. Migratory $CD103^+$ DCs were the only cells able to promote OT-I T cell activation and proliferation (Figure 1I). Altogether, these results demonstrated the unique ability of tumor-infiltrating $CD103^+$ DCs to transport and cross-present tumor-associated antigens to $CD8^+$ T cells in the TdLN, leading to the differentiation of tumor-specific $CD8^+$ T cells.

$CD103^+$ DCs are required to promote anti-PD-L1 Ab- mediated anti-tumor immunity

$CD103^+$ DCs expressed PD-L1 at high levels in the TdLN compared to skin-migratory $CD103^+$ DCs present in the non TdLN (Figure 2A), prompting us to examine whether PD-L1 blockade increases $CD103^+$ DC ability to prime $CD8^+$ T cell in the TdLN and tumor and promotes anti-tumor immunity.

Consistent with prior results (Spranger et al., 2014), PD-L1 blockade given alone or in combination with BRAF inhibition delayed B16 tumor growth (Figures 2B-2C). To investigate the contribution of $CD103^+$ DCs to anti-PD-L1 Ab effect, we compared B16 tumor growth upon PDL1 blockade in wild-type (WT) or *Batf3*$^{-/-}$ mice, which lack $CD103^+$-$CD8^+$ DCs (Figure 2C). Despite the high expression of PD-L1 on B16 tumor cells (Figure 2D), the moderate but significant anti-tumoral effect mediated by PD-L1 blockade was lost in *Batf3*$^{-/-}$ mice. These results established that $CD103^+$ DCs controlled PD-L1 mediated anti-tumor immunity.

PD-L1 blockade fails to significantly promote $CD8^+$ T cell accumulation in the tumor mass

When combined with BRAF inhibitors, PD-L1 blockade delayed tumor growth but failed to prevent tumor relapse after interruption of BRAF inhibition (Figure 2B). While PD-L2 expression increased on tumor migratory $CD103^+$ DCs, its expression was strongly reduced upon BRAF inhibition (Figure S2A), suggesting that the poor tumor response to PD-L1 and BRAF inhibitors was not due to upregulation of PD-L2.

Failure to respond to PD-L1 blockade has been shown to correlate with reduced expression of PD-L1 on tumor-infiltrating immune cells or the absence of $CD8^+$ T cell in the tumor mass prior to treatment (Herbst et al., 2014; Tumeh et al., 2014). While PD-L1 inhibition increased the number of $CD8^+$ T cells producing IFNγ and tumor-necrosis factor (TNF)-α in the TdLN (Figure 2E), the number of $IFN\gamma^+$ $TNF\alpha^+$ $CD8^+$ T cells and the $CD8^+$ T cell over regulatory T cell (Treg) ratio did not significantly increase in anti-PD-L1-treated tumors (Figures 2F-2G). Using tetramers, we quantified antigen presentation in the tumor and LN and observed a slight increase in the priming of tumor-specific $CD8^+$ T cells in both sites (Figure S2B). However, we also found that the tumor-infiltrating T cells remained mostly outside the tumor mass, accumulating mainly within the perivascular areas in the B16 model (Figures 2H-2J). This suggested that defects of T cell recruitment to the tumor site may contribute to the subdued response to anti-PD-L1 Ab. These data contrasted with previous published results showing increased accumulation of intratumoral $CD8^+$ cells in $Braf^{CA}Pten^{loxP}$ tumors treated with BRAF and PD-L1 blockade compared to BRAF blockade alone (Cooper et al., 2014). It is plausible that the additional β-catenin mutation present in our tumor model may have contributed to the limited T cell accumulation in the

Author Manuscript Author Manuscript Author Manuscript Author Manuscript

tumor. This would be consistent with recently published data showing that β-catenin expression in melanoma lesions alters chemokine production thereby compromising DC and T cell recruitment (Spranger et al., 2015).

Flt3 ligand injections dramatically expand CD103$^+$ DC progenitors in the bone marrow and promote their accumulation and proliferation in the tumor mass

We hypothesized that the paucity of CD103$^+$ DCs at the tumor site restricted the expansion of tumor-specific CD8$^+$ T cells and therefore limited anti-PD-L1 Ab anti-tumor efficacy. Another possibility was that the excess of highly phagocytic macrophages competed for antigen availability at the tumor site thereby limiting the ability of CD103$^+$ DCs to prime and activate CD8$^+$ T cells.

To expand CD103$^+$ DCs, we injected mice with the growth factor fms-like tyrosine kinase 3 ligand (Flt3L, referred to hereafter as FL), a cytokine promoting hematopoietic progenitor commitment to the DC lineage as well as DC survival and proliferation in tissues (Liu and Nussenzweig, 2010). We found that 9 daily injections of FL dramatically expanded CD103$^+$ DCs, becoming the predominant myeloid cell population at the tumor site (Figures 3A-3C and 3E). To probe the origin of this dramatic DC expansion in the tumor, we analyzed the FL-induced changes in the bone marrow. We noted an expansion of MHCII^{hi}CD11c$^+$CD103$^-$CD11b$^-$ cells lacking lineage markers (referred to as double negative (DN) cells) in the bone marrow, blood circulation and tumor (Figures 3A and 3E-F). More than 80% of the DN MHCII$^+$CD11c$^+$ cells were positive for Irf8 (Figure 3D), a transcription factor required for the differentiation of CD103$^+$ DCs but not CD11b$^+$ DCs (Ginhoux et al., 2009) and lacked Irf4, the transcription factor required for the differentiation of CD11b$^+$ DCs (Murphy et al., 2013) (Figure 3D). Irf8$^+$ DN cells proliferated actively in the tumor (Figure 3G), suggesting that FL injections led to the expansion of DC progenitors committed to the CD103$^+$ DC lineage and their accumulation at the tumor site. To directly address whether Irf8$^+$ DN cells gave rise to CD103$^+$ DCs, we sorted the DN cells from B16 tumors of FL-treated mice and cultured them in vitro in the presence of FL +/− granulocyte macrophage colony-stimulating factor (GM-CSF) as previously described (Sathe et al., 2011; Schlitzer et al., 2015) (Figure S3A). In FL-supplemented cultures, DN cells gradually differentiated into CD103$^+$CD11b$^-$ DCs, whereas CD11b$^+$ DCs remained unchanged. GM-CSF addition to the cultures further increased DN cell differentiation into CD103$^+$ DCs but failed to promote the differentiation of CD11b$^+$ DCs. This established that the mobilized Irf8$^+$ DN cells were precursors for CD103$^+$ DCs, consistent with the immature CD103$^+$ DCs found *in vivo* in FL-treated tumors (Figure 4A). Altogether these data suggested that FL administration led to the predominant expansion of CD103$^+$ DC progenitors and immature CD103$^+$ DCs at the tumor site.

Flt3 ligand-poly I:C combined therapy significantly enhances the recruitment and activation of effector anti-tumoral CD8$^+$ T cells in melanoma lesions

Immature DCs cannot efficiently prime T cells and therefore we needed to promote the maturation of local FL-mobilized CD103$^+$ DCs. Among APCs, CD103$^+$ DCs and their human counterpart CD141$^+$ DCs uniquely express Toll like receptor 3 (TLR3) (Hashimoto et al., 2011). TLR3 recognizes viral double-stranded RNA and its synthetic analog

Author Manuscript Author Manuscript Author Manuscript Author Manuscript

polyriboinosinic: polyribocytidylic acid (poly I:C, referred to hereafter as pIC) and induces type I IFN production as well as DC maturation via the adaptor protein TRIF (Bogunovic et al., 2011; Bogunovic et al., 2009; Longhi et al., 2009; Matsumoto and Seya, 2008). Production of type I IFN by the $CD103^{+-}$ $CD8^{+}$ DC lineage is required for T cell priming against tumor antigens (Bogunovic et al., 2009; Fuertes et al., 2011). Thus, we chose intratumoral pIC delivery to activate $CD103^{+}$ DCs, increase type I IFN availability at the tumor site and limit potential immune adverse events due to $CD103^{+}$ DC activation in other tissues (Figure S4A).

Poly I:C injections upregulated the expression levels of the costimulatory molecules CD40, CD86 and MHCII on tumor-infiltrating $CD103^{+}$ DCs (Figure 4A) and to a lesser extent on $CD11b^{+}$ DCs (data not shown), indicating proper DC maturation and activation. The significant increase of DC progenitor and mature DC numbers in the tumor mass was accompanied by a significant increase of OVA-specific $IFN\gamma^{+}$ $CD8^{+}$ OT-I cell frequencies in the TdLN of mice injected with B16-OVA tumors and with OT-I cells, compared to control groups (Figure 4B). Combined FL-pIC also led to the expansion of $CD8^{+}$ T cells specific to the melanocyte antigen gp100 in the TdLN of B16 tumor-bearing mice (Figure 4C), suggesting that the combined therapy could also promote the priming and/or expansion of T cells specific for endogenous tumor-associated antigens. Although pIC injections led to reduced B16 tumors lesions compared to PBS injections, FL-pIC significantly enhanced tumor regression compared to either PBS, FL alone or pIC alone -treated tumors (Figure 4D).

Similar to what we observed with B16 tumors, FL-pIC treatment also significantly reduced *Braf*-mutant tumor growth compared to PBS or FL-treated group (Figure 4E). Although not statistically significant, there was a clear trend towards a superior clinical effect in the FL-pIC-treated group compared to the pIC-treated group.

We compared the anti-tumor effect of systemic versus intratumoral injections of pIC and observed, in a dose equivalent manner, a much stronger anti-tumor effect when pIC was administered intratumorally (Figure 4F). Thus intratumoral injections helped lower the pIC dose and reduce its potential toxicity.

As a majority of patients that initially respond to BRAF blockade do relapse (Flaherty et al., 2010), we investigated whether FL-pIC combined treatment increases anti-tumor immunity to melanoma antigens released upon BRAF inhibition therapy and therefore prolongs tumor response to BRAF blockade in mice bearing *Braf*-mutant melanoma lesions (Figure S4B). Similar to B16 tumor-bearing mice, FL-pIC combined therapy enhanced the proliferation of gp100-specific T cells in the TdLN (Figure 4G) and significantly reduced tumor relapse after interruption of BRAF inhibitors compared to control group (Figure 4H).

Therapeutic immunity induced by Flt3L-poly I:C combined therapy requires $CD103^{+}$ DCs and type I IFN

While a slight T cell accumulation was induced upon BRAF inhibition alone, BRAF inhibition combined with FL-pIC treatment promoted a massive T cell infiltration throughout the tumor (Figure 5A-5B). Accordingly, whereas T lymphocytes were almost

Author Manuscript Author Manuscript Author Manuscript Author Manuscript

absent in untreated B16 tumors, FL-pIC increased T cell frequency per mm in the tumor and promoted T cell proliferation in situ (Figures 5C-5E). FL-pIC treatment significantly increased the number of tumor-infiltrating antigen specific cytolytic and IFNγ^+ TNFα^+ CD8$^+$ T cells (Figures 5F-G and Figure S4C) and increased CD8$^+$ T cell/Treg cell ratio at the tumor site (Figure 5H).

Upon injections of the sphingosine 1 phosphate (S1P) receptor antagonist FTY-720, we found a drastic reduction in OT-I cell numbers in the tumor of FL-pIC-treated mice (Figure 5I and Figure S5C). FTY-720 is known to prevent T cell egress from the LN (Figure S5D); therefore, these results could suggest that T cell priming in the TdLN is required to promote the FL-pIC anti-tumor response. Additional experiments will be required to further characterize the contribution of the TdLN versus the tumor site to the induction of anti-tumor immunity.

We then asked whether CD103$^+$ DCs controlled the FL-pIC-mediated anti-tumor effect. B16 tumors injected in *Batf3*$^{-/-}$ animals, which lack CD103$^+$ and CD8$^+$ DCs, did not respond to FL-pIC combined therapy (Figure 5J). Accordingly, effector T cells failed to accumulate in FL-pIC-treated tumors in *Batf3*$^{-/-}$ compared to WT animals (Figure 5K). These results strongly suggested that induction of anti-tumoral effector immunity in FL-pIC-treated mice was dependent on CD103$^+$ DCs.

Depletion of natural killer (NK) cells in FL-pIC-treated mice did not compromise tumor outcome (Figure 5L) indicating that NK cells were dispensable for the FL-pIC-mediated anti-tumor effect. In contrast, depletion of CD4$^+$ and CD8$^+$ T cells prior to FL-pIC injection reduced the FL-pIC therapeutic effect without totally abrogating it (Figure 5L), suggesting that the regression of primary tumors was partially dependent on T cell responses but also on innate immunity induced by CD103$^+$ DCs.

We found that B16 tumors injected into mice lacking the IFN alpha receptor (*Ifnar*$^{-/-}$) failed to respond to FL-pIC therapy (Figure S5A) which was consistent with prior studies showing that type I IFN signature at the tumor site correlates with anti-tumoral immunity (Fuertes et al., 2011). We found that similar to *Ifnar*$^{-/-}$ mice, B16 tumors injected into *Ifnar*$^{-/-}$ bone marrow chimeric animals did not respond to FL-pIC treatment (Figure S5B).

Poly I:C acts through two RNA sensors, TLR3 and melanoma differentiated antigen 5 (MDA5) (Kawai and Akira, 2010). TLR3, which is highly expressed on CD103$^+$ DCs but is lacking on other APCs (Miller et al., 2012), uses TIR domain containing adapter inducing IFNβ (TRIF) for the induction of type I IFN (Kawai and Akira, 2010). We reconstituted mice with bone marrow cells lacking TRIF so that immune cells are unable to respond to TLR3 signaling but should still be able to respond to MDA5. We found that the absence of TLR3-TRIF in immune cells greatly compromised the B16 tumor response to FL-pIC treatment (Figure S5B).

Altogether these data suggested that CD103$^+$ DCs, as well as IFN alpha receptor and TRIF expression in the immune compartment controlled the FL-pIC anti-tumoral effect.

Author Manuscript Author Manuscript Author Manuscript Author Manuscript

Flt3L and poly I:C synergize with anti-PD-L1 Ab treatment to enhance anti-tumor responses to BRAF inhibition

In accordance with previous studies, we found that *in situ* pIC injections substantially increased the expression of PD-L1 on intratumoral $CD103^+$ DCs (Figure 6A), suggesting that PD-L1 upregulation on APCs may limit the therapeutic efficacy of FL-pIC therapy. Thus, we compared the clinical outcome of mice treated with the combined FL-pIC-anti-PD-L1 Ab therapy (referred to as "tritherapy") to mice treated with FL-pIC or anti-PD-L1 Ab alone. The tritherapy dramatically increased the regression of B16 established tumors (Figure 6B). Accordingly, PDL1 inhibition combined to FL-pIC further increased the number of $IFN\gamma^+$ $TNF\alpha^+$ $CD8^+$ T cells in B16 TdLN and tumor and increased the $CD8^+$ T cell/Treg cell ratio in tumors compared to mice treated with FL-pIC or anti-PD-L1 Ab alone (Figures 6C-6E). Treg cells absolute numbers were not decreased but their frequency was reduced due to increased recruitment and proliferation of $CD8^+$ T effector cells (data not shown).

The improved clinical outcome of B16 tumors treated with the tritherapy prompted us to test whether it could be used to further reduce the relapse of *Braf*-mutant lesions after interruption of BRAF inhibition. Whereas tumor growth was delayed but not abrogated in control groups treated with anti-PD-L1 Ab or FL-pIC alone, *Braf*-mutant lesions treated with the tritherapy were strongly reduced upon interruption of BRAF blockade (Figure 6F).

We then probed the tritherapy effect on secondary tumors that developed upon tumor rechallenge induced through 4-HT re-administration. Since the secondary tumors did not receive any treatment, their regression should depend on a memory anti-tumor immune response induced upon treatment of the primary tumors. Thus, mice harboring *Braf*-mutant tumors were treated with the tritherapy, anti-PD-L1 Ab alone or immunoglobulin G (IgG)-PBS, in addition to BRAF inhibition, as in Figure 6F. Ten days after treatment interruption, mice were rechallenged with 4-HT on the opposite flank of the treated primary tumors and analyzed one month later (Figure S6A). Mice in which the primary tumors were treated with the tritherapy developed much smaller secondary tumors accompanied with increased accumulation of $IFN\gamma^+$ $TNF\alpha^+$ $CD8^+$ T cells in the TdLN along with massive T cell accumulation in the tumors compared to mice treated initially with anti-PD-L1 alone or isotype control (Figures 6G-6J). PD-L1 inhibition alone did not confer superior protective immunity compared to non-treated animals (Figures 6G-6J).

Tyr::CreER;$Braf^{CA}$/$Pten^{loxP}$/$Ctnnb1^{loxex3}$ transgenic mice develop serial skin tumors on ears, eyes, paws and tail within 2 months after primary tumor induction with 4-HT. These secondary tumors could represent either skin metastases or tumors that form due to leakiness of the cretransgene. Consistent with our findings upon tumor rechallenge, mice in which the primary tumors were treated with the tritherapy in addition to BRAF inhibition had significantly reduced skin tumors (Figure 6K) compared to mice treated with anti-PD-L1 Ab combined with BRAF inhibitors. This was dependent on T cell immunity as T cell depletion abrogated the clinical benefit of tritherapy on the development of secondary tumors (Figures 6I and 6K).

Author Manuscript Author Manuscript Author Manuscript Author Manuscript

Altogether, these data showed that FL and pIC synergized with PD-L1 blockade to prevent the relapse of *Braf*-mutant melanoma lesions after BRAF inhibition and to protect from tumor rechallenge.

DISCUSSION

In the present study we found that while most tumor-infiltrating myeloid cells could capture tumor antigens in two mouse melanoma models, tumor-infiltrating $CD103^+$ DCs were uniquely able to transport intact antigens to the TdLN and prime tumor-specific LN $CD8^+$ T cells. $CD103^+$ DCs controlled anti-PD-L1 Ab- mediated anti-tumor immunity, however PD-L1 inhibition led to modest anti-tumor response and this response was dramatically increased upon expansion and activation of $CD103^+$ DC at the tumor site.

Our findings that intratumoral $CD103^+$ DCs are uniquely able to transport intact antigens to the TdLN are consistent with the low expression levels of lysosomal degradative enzymes (Miller et al., 2012; Savina et al., 2006) and in line with our previous results showing that lung resident $CD103^+$ DCs are uniquely able to transport intact viral antigens to the LN upon lung infection with influenza virus (Helft et al., 2012). These results are also in accordance with prior studies showing the requirement for $CD103^+$ DCs in the induction of therapeutic immunity against fibrosarcoma tumor grafts (Hildner et al., 2008).

The low numbers of $CD8^+$ T cells present in B16 and *Braf*-mutant tumors and their limited accumulation upon BRAF and/or PD-L1 blockade may explain the reduced clinical response to these treatments as previously suggested (Chen and Mellman, 2013; Gajewski et al., 2013). Using an experimental model of breast cancer, recent results revealed that accumulation and activation of intratumoral $CD8^+$ T effector cells is dependent on intratumoral $CD103^+$ DCs (Broz et al., 2014) suggesting that the limited infiltration of $CD8^+$ T cells observed in B16 and *Braf*-mutant lesions may be a consequence of the reduced accumulation of $CD103^+$ DCs in tumors. We have previously reported that tissue resident $CD103^+$ DCs fail to accumulate in injured tissues (Helft et al., 2012), which may explain the limited numbers of $CD103^+$ DCs in tumors. We discovered that FL injections promoted the differentiation of $CD103^+$ DC progenitors already in the bone marrow and their expansion at the tumor site. FL ability to instruct DC progenitors commitment mainly to the $CD103^+$ DC lineage, although unexpected, is consistent with increased FL receptor expression on $CD103^+$ DCs compared to $CD11b^+$ DCs (Liu and Nussenzweig, 2010; Miller et al., 2012) and suggests that increased Flt3 signaling might enforce IRF8 signaling thereby promoting $CD103^+$ DC differentiation.

The expansion of $CD103^+$ DC progenitors was associated with a substantial accumulation of immature $CD103^+$ DCs at the tumor site, which became the predominant myeloid cell population in FL-treated tumors and may explain the increased accumulation of Treg cells in FL-treated tumors and the limited ability of FL to improve tumor response. These results caution the use of FL without a DC maturation agent in tumor patients. Addition of intratumoral pIC significantly increased tumor-specific $CD8^+$ T cells activation in the TdLN and their accumulation at the tumor site, improving the regression of B16 and *Braf*-mutant tumors. T cells partly controlled the regression of primary tumors and were essential for the

Author Manuscript Author Manuscript Author Manuscript Author Manuscript

reduction of secondary *Braf*-mutant melanoma lesions that developed either spontaneously after the primary tumor or upon tumor rechallenge, suggesting that the tritherapy synergized with BRAF inhibitors to promote a strong and efficient anti-tumor memory T cell immune response that prevented the growth of tumors. The presence of the human $CD103^+$ DC equivalent, $CD141^+$ DCs, correlates with better outcome in human tumors (Sluijter et al., 2015). Similar to mouse $CD103^+$ DCs, human $CD141^+$ DCs express IRF8, high levels of FLT3 and TLR3, and pIC activation of human $CD141^+$ cells leads to the upregulation of PD-L1 (Bogunovic et al., 2011) and to their increased cross-priming of $CD8^+$ T cells (Crozat et al., 2010; Jongbloed et al., 2010; Poulin et al., 2010). This suggests that FL-pIC-anti-PD-L1 Ab tritherapy should help expand and activate tumor-infiltrating DCs and promote the induction of tumor-specific $CD8^+$ T cell immunity in cancer patients.

The introduction of combination chemotherapy in the 1960s dramatically improved the clinical outcome of numerous tumors compared to monotherapic regimen (Frei et al., 1958). Our results support the need of novel immunotherapy combination strategies to maximize the induction, expansion, recruitment and cytotoxic function of tumor-specific $CD8^+$ T cells. We believe that the use of FL to expand $CD103^+$ DC progenitors at the tumor site followed by intratumoral pIC to induce type I IFN release in the tumor and promote DC immunogenic function, has the potential to transform clinical response to anti-PD-L1 treatment in cancer patients.

EXPERIMENTAL PROCEDURES

Mice

C57BL/6 ($CD45.2^+$) and congenic $CD45.1^+$ C57BL/6 mice were purchased from Frederick Cancer Research Center or Charles River Laboratories. Tyr::CreER;$Braf^{CA}$/$Pten^{loxP}$/$Ctnnb1^{loxex3}$ transgenic mice were obtained from Dr. Marcus Bosenberg (Yale University) (Damsky et al., 2011). Tyr::CreER;$Braf^{CA}$/$Pten^{loxP}$ mice were purchased from Jackson laboratories and crossed to C57BL/6 tdTomato reporter mice (Jackson laboratories, B6.Cg-Gt (ROSA)26$Sor^{tm14(CAG-tdTomato)Hze}$ /J).

Tumor induction

The C57BL/6 derived melanoma cell lines B16 (Mayordomo et al., 1995), the B16-OVA-transfected clone and B16YFP–transfected clone were maintained at 37°C with 5% CO_2 in RPMI supplemented with 10% heat-inactivated FCS, penicillin and streptomycin (Cellgro). 3.10^5 tumor cells were injected s.c. in 50µl PBS on the flank. *Braf*-mutant melanoma lesions were induced by topical application of 1µl of 5 mM 4-hydroxytamoxifen. Tumor size was determined by the formula L*W*D where L=length, W=width and D=depth, on the indicated days.

Treatments

Flt3L (30 µg in 100 µl PBS; Celldex) or control PBS was injected intraperitoneally (9 daily injections, unless otherwise noted). High molecular weight poly I:C (50µg in 50µl; Invivogen) was injected intratumorally. For BRAF inhibition, mice were fed by a chow diet containing 417mg/kg PLX4720 (Plexxikon) for 4 days or control diet.

Author Manuscript Author Manuscript Author Manuscript Author Manuscript

Preparation of cell suspensions

Single cell suspension was obtained after tumor digestion with 400U/ml of type D collagenase (Roche) at 37°C for 1h. Hematopoietic cells were enriched by density gradient centrifugation with 40/90 Percoll (GE Healthcare Life Sciences) for 30 min at 2500 rpm, before a 1min-incubation with RBC lysis buffer (Biolegend) at RT. DCs were obtained from LN after incubation with 400 U/ml Collagenase D (Roche) for 25 min at 37°C. In some cases, DC enrichment was performed with CD11c microbeads following manufacturer's instructions (Miltenyi Biotec).

FTY-720 treatment

FTY-720 was purchased from Sigma, and injected i.p. (200μl) at a final concentration of 100μg/ml in saline every day over the indicated time periods.

Re-stimulation and intracellular cytokine staining

Cells were stimulated with 100 ng/ml PMA (Sigma) and 0.5 mg/ml ionomycin (Sigma-Aldrich) at 37°C for 3 hrs, in the presence of Brefeldin A (10 μg/ml; Sigma) to allow accumulation of intracellular cytokines. After staining of surface markers, cells were fixed and permeabilized, followed by staining of IFNγ, TNFα and Foxp3.

In vivo killing assay

Five days after the last injection of FL and pIC, mice were injected i.v. with spleen cells differentially labeled with 20 or 200 nM CFSE (Invitrogen) and loaded with 10 or 100 nM ovalbumin$_{257–264}$ (referred to as OT-I peptide), respectively. Tumors were collected 24h after injection of target cells. Percentage of OVA-specific killing was calculated as described elsewhere (Hermans et al., 2004).

Antibody treatment

Groups of mice were injected with 200 μg anti-CD8 (2.43), CD4 (GK1.5), or NK (PK136)-specific mAb or Rat IgG (Sigma), 3 times at 2 days interval, starting 2 days before B16 tumor cell injection, followed by a 200 μg dose every 7 d. For PD-L1 blockade, mice were injected i.p. with 3 doses of 200 μg every other day of anti-PD-L1 (10F.9G2, BioXCell)-specific mAb or Rat IgG (Sigma).

Statistical analysis

Graphs were compiled and statistical analyses were performed using Prism software (GraphPad). Statistical significance was evaluated with unpaired t-test when comparing two groups and one-way ANOVA when comparing more than 2 groups. In all cases, p values < 0.05 were considered statistically significant.

Supplementary Material

Refer to Web version on PubMed Central for supplementary material.

Author Manuscript Author Manuscript Author Manuscript Author Manuscript

ACKNOWLEDGEMENTS

MM was supported by NIH grant R01 CA154947A, R01CA190400, R01 CA173861, U01AI095611, R01AI104848. H.S. was supported by a postdoctoral fellowship from the Association pour la Recherche contre le Cancer and by the Irvington postdoctoral fellowship of the Cancer Research Institute. We thank Jill Gregory, Manager of Academic Medical Illustration (Icahn School of Medicine at Mount Sinai) for the graphical abstract.

REFERENCES

Bogunovic D, Manches O, Godefroy E, Yewdall A, Gallois A, Salazar AM, Marie I, Levy DE, Bhardwaj N. TLR4 engagement during TLR3-induced proinflammatory signaling in dendritic cells promotes IL-10-mediated suppression of antitumor immunity. Cancer research. 2011; 71:5467–5476.

Bogunovic D, O'Neill DW, Belitskaya-Levy I, Vacic V, Yu YL, Adams S, Darvishian F, Berman R, Shapiro R, Pavlick AC, et al. Immune profile and mitotic index of metastatic melanoma lesions enhance clinical staging in predicting patient survival. Proceedings of the National Academy of Sciences of the United States of America. 2009; 106:20429–20434. [PubMed: 19915147]

Broz ML, Binnewies M, Boldajipour B, Nelson AE, Pollack JL, Erle DJ, Barczak A, Rosenblum MD, Daud A, Barber DL, et al. Dissecting the tumor myeloid compartment reveals rare activating antigen-presenting cells critical for T cell immunity. Cancer cell. 2014; 26:638–652.

Chen DS, Mellman I. Oncology meets immunology: the cancer-immunity cycle. Immunity. 2013; 39:1–10.

Cooper ZA, Juneja VR, Sage PT, Frederick DT, Piris A, Mitra D, Lo JA, Hodi FS, Freeman GJ, Bosenberg MW, et al. Response to BRAF inhibition in melanoma is enhanced when combined with immune checkpoint blockade. Cancer immunology research. 2014; 2:643–654.

Crozat K, Guiton R, Contreras V, Feuillet V, Dutertre CA, Ventre E, Vu Manh TP, Baranek T, Storset AK, Marvel J, et al. The XC chemokine receptor 1 is a conserved selective marker of mammalian cells homologous to mouse CD8alpha+ dendritic cells. The Journal of experimental medicine. 2010; 207:1283–1292. [PubMed: 20479118]

Damsky WE, Curley DP, Santhanakrishnan M, Rosenbaum LE, Platt JT, Gould Rothberg BE, Taketo MM, Dankort D, Rimm DL, McMahon M, Bosenberg M. beta-catenin signaling controls metastasis in Braf-activated Pten-deficient melanomas. Cancer cell. 2011; 20:741–754.

Fife BT, Pauken KE, Eagar TN, Obu T, Wu J, Tang Q, Azuma M, Krummel MF, Bluestone JA. Interactions between PD-1 and PD-L1 promote tolerance by blocking the TCR-induced stop signal. Nature immunology. 2009; 10:1185–1192.

Flaherty KT, Puzanov I, Kim KB, Ribas A, McArthur GA, Sosman JA, O'Dwyer PJ, Lee RJ, Grippo JF, Nolop K, Chapman PB. Inhibition of mutated, activated BRAF in metastatic melanoma. The New England journal of medicine. 2010; 363:809–819. [PubMed: 20818844]

Forster R, Schubel A, Breitfeld D, Kremmer E, Renner-Muller I, Wolf E, Lipp M. CCR7 coordinates the primary immune response by establishing functional microenvironments in secondary lymphoid organs. Cell. 1999; 99:23–33.

Frei E 3rd, Holland JF, Schneiderman MA, Pinkel D, Selkirk G, Freireich EJ, Silver RT, Gold GL, Regelson W. A comparative study of two regimens of combination chemotherapy in acute leukemia. Blood. 1958; 13:1126–1148. [PubMed: 13596417]

Fuertes MB, Kacha AK, Kline J, Woo SR, Kranz DM, Murphy KM, Gajewski TF. Host type I IFN signals are required for antitumor CD8+ T cell responses through CD8{alpha}+ dendritic cells. The Journal of experimental medicine. 2011; 208:2005–2016. [PubMed: 21930765]

Gajewski TF, Woo SR, Zha Y, Spaapen R, Zheng Y, Corrales L, Spranger S. Cancer immunotherapy strategies based on overcoming barriers within the tumor microenvironment. Current opinion in immunology. 2013; 25:268–276. [PubMed: 23579075]

Galon J, Costes A, Sanchez-Cabo F, Kirilovsky A, Mlecnik B, Lagorce-Pages C, Tosolini M, Camus M, Berger A, Wind P, et al. Type, density, and location of immune cells within human colorectal tumors predict clinical outcome. Science. 2006; 313:1960–1964.

Author Manuscript Author Manuscript Author Manuscript Author Manuscript

Ginhoux F, Liu K, Helft J, Bogunovic M, Greter M, Hashimoto D, Price J, Yin N, Bromberg J, Lira SA, et al. The origin and development of nonlymphoid tissue CD103+ DCs. J Exp Med. 2009; 206:3115–3130. [PubMed: 20008528]

Guilliams M, Ginhoux F, Jakubzick C, Naik SH, Onai N, Schraml BU, Segura E, Tussiwand R, Yona S. Dendritic cells, monocytes and macrophages: a unified nomenclature based on ontogeny. Nature reviews. Immunology. 2014; 14:571–578.

Hashimoto D, Miller J, Merad M. Dendritic cell and macrophage heterogeneity in vivo. Immunity. 2011; 35:323–335.

Helft J, Manicassamy B, Guermonprez P, Hashimoto D, Silvin A, Agudo J, Brown BD, Schmolke M, Miller JC, Leboeuf M, et al. Cross-presenting CD103+ dendritic cells are protected from influenza virus infection. The Journal of clinical investigation. 2012; 122:4037–4047. [PubMed: 23041628]

Herbst RS, Soria JC, Kowanetz M, Fine GD, Hamid O, Gordon MS, Sosman JA, McDermott DF, Powderly JD, Gettinger SN, et al. Predictive correlates of response to the anti-PD-L1 antibody MPDL3280A in cancer patients. Nature. 2014; 515:563–567. [PubMed: 25428504]

Hermans IF, Silk JD, Yang J, Palmowski MJ, Gileadi U, McCarthy C, Salio M, Ronchese F, Cerundolo V. The VITAL assay: a versatile fluorometric technique for assessing CTL- and NKT-mediated cytotoxicity against multiple targets in vitro and in vivo. Journal of immunological methods. 2004; 285:25–40. [PubMed: 14871532]

Hildner K, Edelson BT, Purtha WE, Diamond M, Matsushita H, Kohyama M, Calderon B, Schraml BU, Unanue ER, Diamond MS, et al. Batf3 deficiency reveals a critical role for CD8alpha+ dendritic cells in cytotoxic T cell immunity. Science. 2008; 322:1097–1100.

Jongbloed SL, Kassianos AJ, McDonald KJ, Clark GJ, Ju X, Angel CE, Chen CJ, Dunbar PR, Wadley RB, Jeet V, et al. Human CD141+ (BDCA-3)+ dendritic cells (DCs) represent a unique myeloid DC subset that cross-presents necrotic cell antigens. The Journal of experimental medicine. 2010; 207:1247–1260. [PubMed: 20479116]

Kawai T, Akira S. The role of pattern-recognition receptors in innate immunity: update on Toll-like receptors. Nature immunology. 2010; 11:373–384.

Keir ME, Butte MJ, Freeman GJ, Sharpe AH. PD-1 and its ligands in tolerance and immunity. Annual review of immunology. 2008; 26:677–704.

Kroemer G, Galluzzi L, Kepp O, Zitvogel L. Immunogenic cell death in cancer therapy. Annual review of immunology. 2013; 31:51–72.

Liu K, Nussenzweig MC. Origin and development of dendritic cells. Immunological reviews. 2010; 234:45–54.

Longhi MP, Trumpfheller C, Idoyaga J, Caskey M, Matos I, Kluger C, Salazar AM, Colonna M, Steinman RM. Dendritic cells require a systemic type I interferon response to mature and induce CD4+ Th1 immunity with poly IC as adjuvant. The Journal of experimental medicine. 2009; 206:1589–1602. [PubMed: 19564349]

Matsumoto M, Seya T. TLR3: interferon induction by double-stranded RNA including poly(I:C). Advanced drug delivery reviews. 2008; 60:805–812. [PubMed: 18262679]

Mayordomo JI, Zorina T, Storkus WJ, Zitvogel L, Celluzzi C, Falo LD, Melief CJ, Ildstad ST, Kast WM, Deleo AB, et al. Bone marrow-derived dendritic cells pulsed with synthetic tumour peptides elicit protective and therapeutic antitumour immunity. Nature medicine. 1995; 1:1297–1302.

Merad M, Sathe P, Helft J, Miller J, Mortha A. The dendritic cell lineage: ontogeny and function of dendritic cells and their subsets in the steady state and the inflamed setting. Annual review of immunology. 2013; 31:563–604.

Miller JC, Brown BD, Shay T, Gautier EL, Jojic V, Cohain A, Pandey G, Leboeuf M, Elpek KG, Helft J, et al. Deciphering the transcriptional network of the dendritic cell lineage. Nat Immunol. 2012; 13:888–899.

Murphy TL, Tussiwand R, Murphy KM. Specificity through cooperation: BATF-IRF interactions control immune-regulatory networks. Nature reviews. Immunology. 2013; 13:499–509.

Page DB, Postow MA, Callahan MK, Allison JP, Wolchok JD. Immune modulation in cancer with antibodies. Annual review of medicine. 2014; 65:185–202.

Poulin LF, Salio M, Griessinger E, Anjos-Afonso F, Craciun L, Chen JL, Keller AM, Joffre O, Zelenay S, Nye E, et al. Characterization of human DNGR-1+ BDCA3+ leukocytes as putative equivalents

Author Manuscript Author Manuscript Author Manuscript Author Manuscript

of mouse CD8alpha+ dendritic cells. The Journal of experimental medicine. 2010; 207:1261–1271. [PubMed: 20479117]

Salmon H, Franciszkiewicz K, Damotte D, Dieu-Nosjean MC, Validire P, Trautmann A, Mami-Chouaib F, Donnadieu E. Matrix architecture defines the preferential localization and migration of T cells into the stroma of human lung tumors. The Journal of clinical investigation. 2012; 122:899–910. [PubMed: 22293174]

Sathe P, Pooley J, Vremec D, Mintern J, Jin JO, Wu L, Kwak JY, Villadangos JA, Shortman K. The acquisition of antigen cross-presentation function by newly formed dendritic cells. J Immunol. 2011; 186:5184–5192.

Savina A, Jancic C, Hugues S, Guermonprez P, Vargas P, Moura IC, Lennon-Dumenil AM, Seabra MC, Raposo G, Amigorena S. NOX2 controls phagosomal pH to regulate antigen processing during crosspresentation by dendritic cells. Cell. 2006; 126:205–218.

Schlitzer A, Sivakamasundari V, Chen J, Sumatoh HR, Schreuder J, Lum J, Malleret B, Zhang S, Larbi A, Zolezzi F, et al. Identification of cDC1- and cDC2-committed DC progenitors reveals early lineage priming at the common DC progenitor stage in the bone marrow. Nature immunology. 2015; 16:718–728.

Sharma P, Allison JP. The future of immune checkpoint therapy. Science. 2015a; 348:56–61. [PubMed: 25838373]

Sharma P, Allison JP. Immune checkpoint targeting in cancer therapy: toward combination strategies with curative potential. Cell. 2015b; 161:205–214. [PubMed: 25860605]

Sluijter BJ, van den Hout MF, Koster BD, van Leeuwen PA, Schneiders FL, van de Ven R, Molenkamp BG, Vosslamber S, Verweij CL, van den Tol MP, et al. Arming the Melanoma Sentinel Lymph Node through Local Administration of CpG-B and GM-CSF: Recruitment and Activation of BDCA3/CD141+ Dendritic Cells and Enhanced Cross-Presentation. Cancer immunology research. 2015; 3:495–505.

Spranger S, Bao R, Gajewski TF. Melanoma-intrinsic beta-catenin signalling prevents anti-tumour immunity. Nature. 2015; 523:231–235.

Spranger S, Koblish HK, Horton B, Scherle PA, Newton R, Gajewski TF. Mechanism of tumor rejection with doublets of CTLA-4, PD-1/PD-L1, or IDO blockade involves restored IL-2 production and proliferation of CD8(+) T cells directly within the tumor microenvironment. Journal for immunotherapy of cancer. 2014; 2:3.

Tumeh PC, Harview CL, Yearley JH, Shintaku IP, Taylor EJ, Robert L, Chmielowski B, Spasic M, Henry G, Ciobanu V, et al. PD-1 blockade induces responses by inhibiting adaptive immune resistance. Nature. 2014; 515:568–571.

Yokosuka T, Takamatsu M, Kobayashi-Imanishi W, Hashimoto-Tane A, Azuma M, Saito T. Programmed cell death 1 forms negative costimulatory microclusters that directly inhibit T cell receptor signaling by recruiting phosphatase SHP2. The Journal of experimental medicine. 2012; 209:1201–1217.

Author Manuscript Author Manuscript Author Manuscript Author Manuscript

HIGHLIGHTS

- $CD103^+$ DCs uniquely transport intact antigen to the TdLN and prime $CD8^+$ T cells
- $CD103^+$ DCs are required to induce anti-PD-L1 Ab- mediated anti-tumor immunity
- Flt3L-poly I:C induces expansion and activation of $CD103^+$ DC progenitors in tumors
- Flt3L-poly I:C therapy enhances tumor responses to BRAF and checkpoint blockade

Author Manuscript Author Manuscript Author Manuscript Author Manuscript

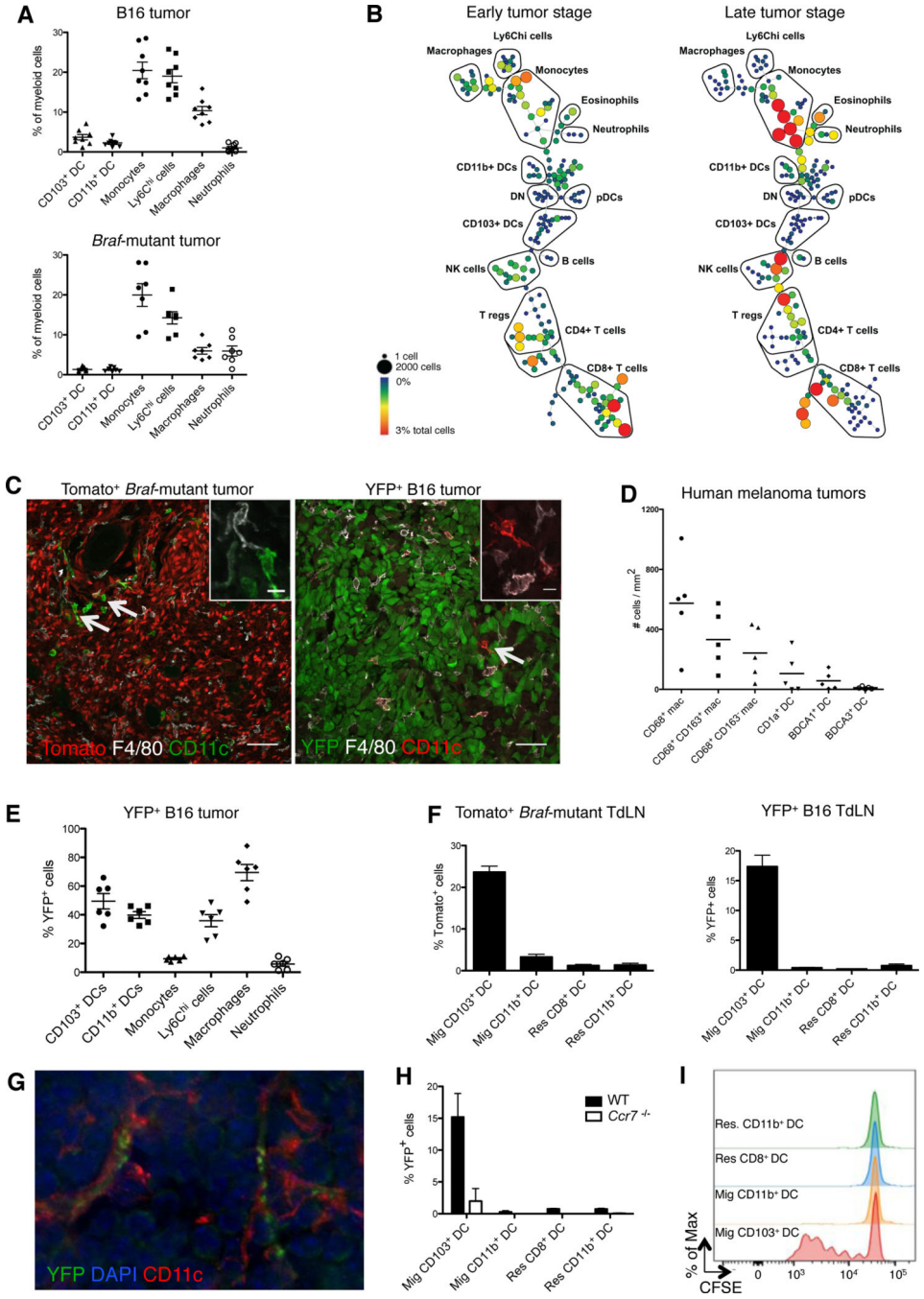

Figure 1. CD103$^+$ DCs uniquely transport intact antigens to the tumor-draining lymph nodes

B16 and *Braf*-mutant tumors and LN were analyzed at day 15 and 25, respectively, unless specified otherwise.

(A) Frequency of each myeloid cell population among total myeloid cells infiltrating B16 (n=8) and *Braf*-mutant tumors (n=7). See Figure S1A for gating strategy. Shown is the mean ± SEM of 2-3 independent experiments.

Author Manuscript Author Manuscript Author Manuscript Author Manuscript

(B) CyTOF analysis of tumor-infiltrating immune cells at early (day 10) and late (day 16) stages of B16 tumor growth. Gated live $CD45^+$ cells were clustered using SPADE based on 27 markers. Trees are representative of 2 experiments with similar results.

(C) Representative confocal images showing $CD11c^+$ $F4/80^-$ DCs and macrophage/monocyte-derived $CD11c^{+/-}$ $F4/80^+$ cells in $Tomato^+$ *Braf*-mutant and B16-YFP tumors, scale bar: 50μm. The right upper corners show magnification of a DC and a macrophage/monocyte-derived cell, scale bar: 10μm. Arrows show rare tumor-infiltrating DCs.

(D) Density of macrophages and DCs infiltrating human melanoma primary tumors (n=5) quantified from tumor sections stained using multiplexed immunohistochemistry (Figure S1D).

(E) Frequency of YFP^+ cells infiltrating B16-YFP tumors. Shown is the mean ± SEM of 2 independent experiments (n=6).

(F) Frequency of $Tomato^+$ and YFP^+ cells in skin migratory ($CD11c^+MHCII^{hi}$) and LN-resident ($CD11c^{hi}MHCII^+$) DCs in the LN draining $Tomato^+$ *Braf*-mutant (left panel, n=9) and B16-YFP tumors (right panel, n=12). Shown are the mean ± SEM of 4 independent experiments.

(G) Representative image of a $CD11c^+$ cell harboring YFP^+ vesicles in the LN draining B16-YFP tumors.

(H) Frequency of YFP^+ cells among migratory DCs isolated from the LN draining B16-YFP tumors in WT or $Ccr7^{-/-}$ mice (n=2).

(I) Migratory and LN resident DCs were sorted from the LN draining B16-OVA tumors and co-cultured with CFSE-labeled OT-I T cells (DC-T ratio = 1/3). Three days later, the proliferation of OT-I T cells was determined by CFSE dilution. Histograms represent one of two independent experiments with similar results.

See also Figure S1.

Author Manuscript Author Manuscript Author Manuscript Author Manuscript

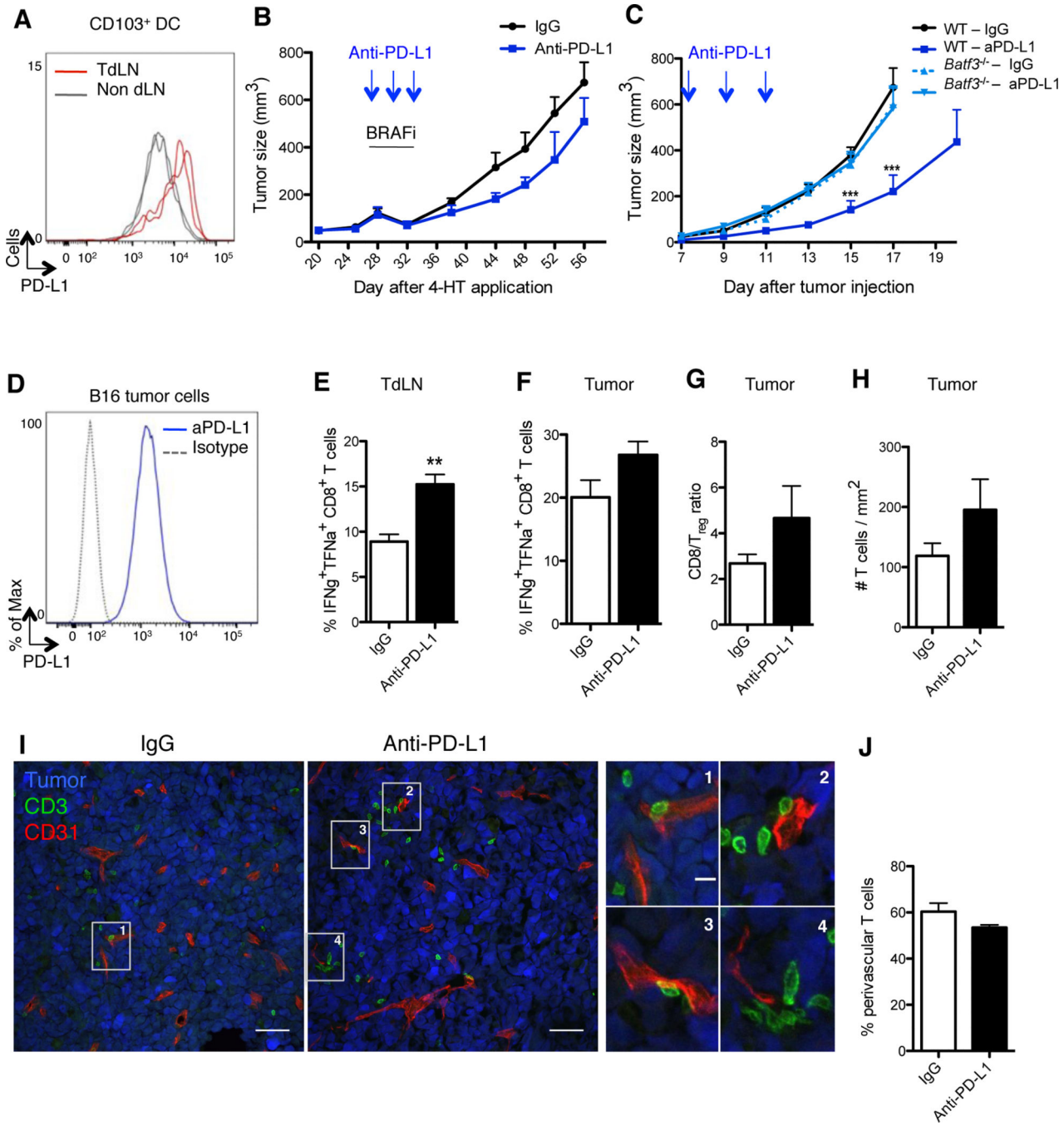

Figure 2. CD103$^+$ DCs control tumor response to PD-L1 blockade

(A) PD-L1 expression on CD103$^+$ DCs purified from B16 TdLN (red lines) and non-draining LN (grey lines), day 15 after tumor challenge. Representative flow cytometry histogram of 2 experiments.

(B) *Braf*-mutant mice were treated i.p. with either anti-PD-L1 or a control mAb on days 28 (tumor size: 100-150μm^3), 30 and 32 after 4-HT topical application. All mice were treated with BRAF inhibitors from day 28 to 32. Shown is mean ± SEM of 2 independent experiments (n= 5-6).

Author Manuscript Author Manuscript Author Manuscript Author Manuscript

(C) B16 tumor-bearing WT or *Batf3*$^{-/-}$ mice were treated i.p. with either anti-PD-L1 or a control mAb on days 7, 9 and 11 after tumor challenge. Tumor growth was followed for 17-20 days. Shown is the mean ± SEM of 2 independent experiments (n=5-8).
(D) PD-L1 expression on cultured B16 tumor cells.
(E-J) Mice were inoculated with B16 tumor cells and treated as in (C).
(E-F) On day 15 mice were sacrificed and CD8$^+$ T cells from TdLN (E) or tumor (F) were analyzed for the production of IFNγ and TNFα following 3-hr PMA/ionomycin stimulation. Shown is the mean ± SEM of 2 independent experiments (n= 4-5 mice).
(G) CD8$^+$ T cell/Treg cell ratio 15 days after tumor challenge is shown as the mean ± SEM of 2 independent experiments (n=4-5).
(H) B16-YFP tumors were harvested on day13 (2 days after the last injection of anti-PD-L1 or control mAb) and stained with anti-CD3 mAb. The density of CD3$^+$ T cells infiltrating B16-YFP tumors was automatically quantified with Cell Profiler software from confocal images. Shown is the mean ± SEM of 3 independent experiments (n=4-6). 12-16 tiled 20x images were analyzed per animal.
(I) B16-YFP tumors (here in blue) were harvested and frozen on day 13 and stained with for T cells (CD3$^+$, green) and blood vessels (CD31$^+$, red). Panels show confocal images (scale bar: 50μm) representative of 3 experiments with similar results. Right panels show higher magnifications of T cells surrounding vessels (scale bar: 10μm).
(J) As in (I), but the percentages of CD3$^+$ T cells found in perivascular areas (≤30μm from a CD31$^+$ vessel) were quantified using Cell Profiler software. Shown is the mean ± SEM of 3 independent experiments (n=4-6).
See also Figure S2.

Author Manuscript Author Manuscript Author Manuscript Author Manuscript

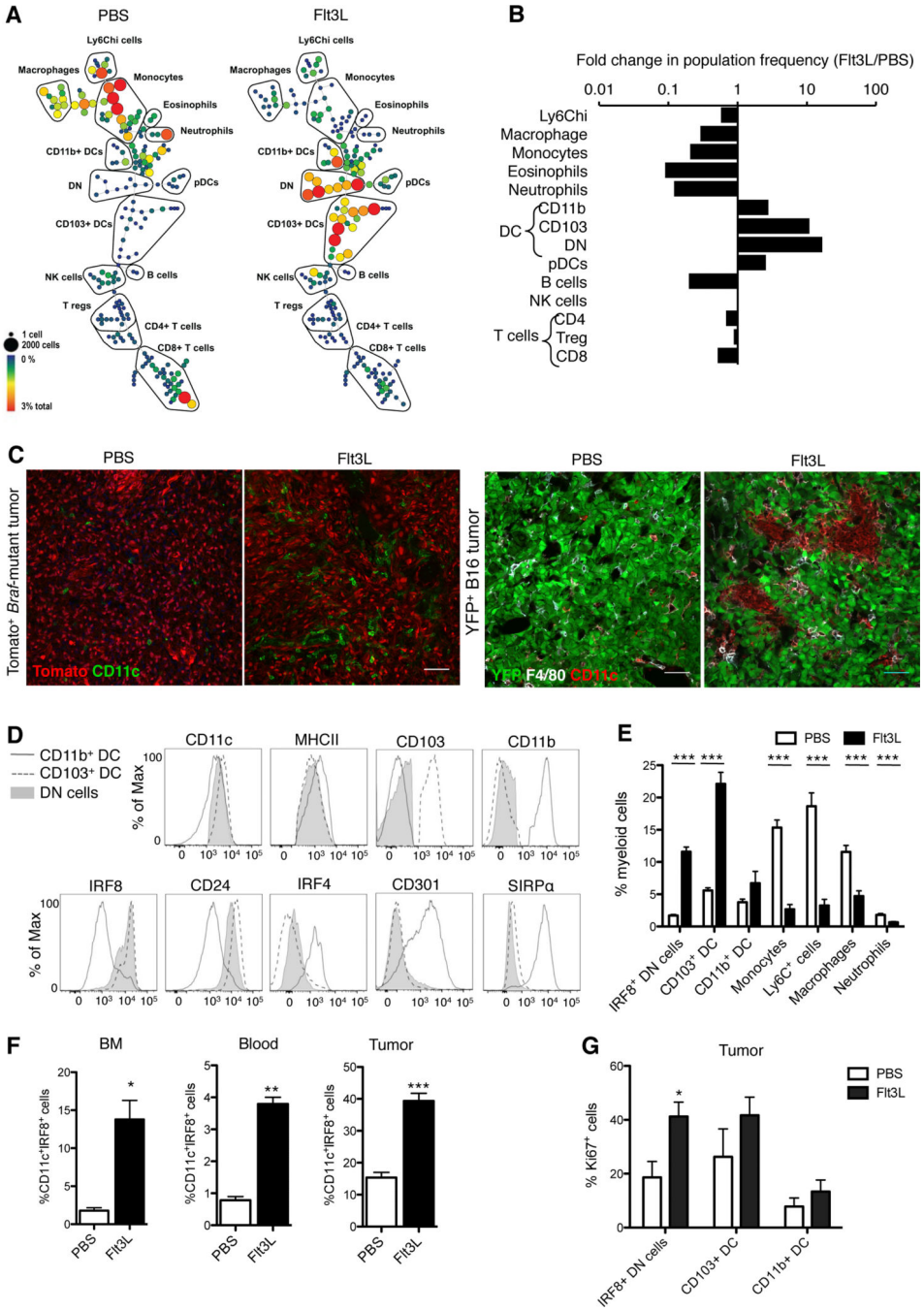

Figure 3. Flt3L injections dramatically expand CD103$^+$ DC progenitors in the bone marrow and promote their accumulation and expansion in the tumor mass

(A) CyTOF analysis of tumor-infiltrating immune cells on day 13 after B16 tumor challenge in mice treated i.p. for 9 consecutive days starting at day 3 post tumor injection with 30μg FL or PBS. SPADE trees were colored by relative population frequency out of total live CD45$^+$ cells. Five mice were pooled to build each SPADE tree. Trees are representative of 2 experiments with similar results.

(B) Fold changes in relative frequency of immune cell populations (identified by SPADE clustering performed in A) between FL- and PBS-treated mice.

Author Manuscript Author Manuscript Author Manuscript Author Manuscript

(C) Representative confocal images of DCs infiltrating tomato$^+$ *Braf*-mutant tumors (red) and B16-YFP tumors (green) treated with 9 daily injections of FL or PBS starting on day 18 after 4-HT topical application (*Braf*-mutant) or 3 days after tumor challenge (B16). Tumor biopsies were isolated and frozen 30 days (*Braf*-mutant) and 15 days (B16) after tumor challenge. In *Braf*-mutant tumors, DCs were identified as CD11c$^+$ cells (green) whereas in B16 tumor DCs were identified as F4/80$^-$CD11c$^+$ (red). Scale bar: 50μm.

(D) Mice were treated as in A. Histograms show the expression of cell surface markers or transcription factors in CD103$^+$ DCs (dashed line), CD11b$^+$ DCs (grey line) and MHCII^{hi}CD11c$^+$Ly6C$^-$CD64$^-$CD103$^-$CD11b$^-$ double negative cells (DN: full grey) infiltrating B16 tumors on day 13 after tumor challenge. Results shown are representative histograms of 2 experiments.

(E) Frequency of myeloid cell populations infiltrating B16 tumors in mice treated with FL or PBS as in A. Results shown are the mean ± SEM of 3 independent experiments with a total of 8 mice.

(F) Frequency of MHCII^{hi}CD11c$^+$Ly6C$^-$CD64$^-$CD103$^-$CD11b$^-$IRF8$^+$ (IRF8$^+$ DN) cells in bone marrow (BM), blood and tumors of B16 tumor-bearing mice analyzed 2 days after 9 daily injections of FL or PBS. Shown is the mean ± SEM of one experiment (n=5).

(G) Frequency of Ki67$^+$ cells among IRF8$^+$ DN cells, CD103$^+$ DCs and CD11b$^+$ DCs infiltrating B16 tumors site analyzed 2 days after 9 daily injections of FL or PBS. Shown is the mean ± SEM of 2 independent experiments (n=4).

See also Figure S3.

Author Manuscript Author Manuscript Author Manuscript Author Manuscript

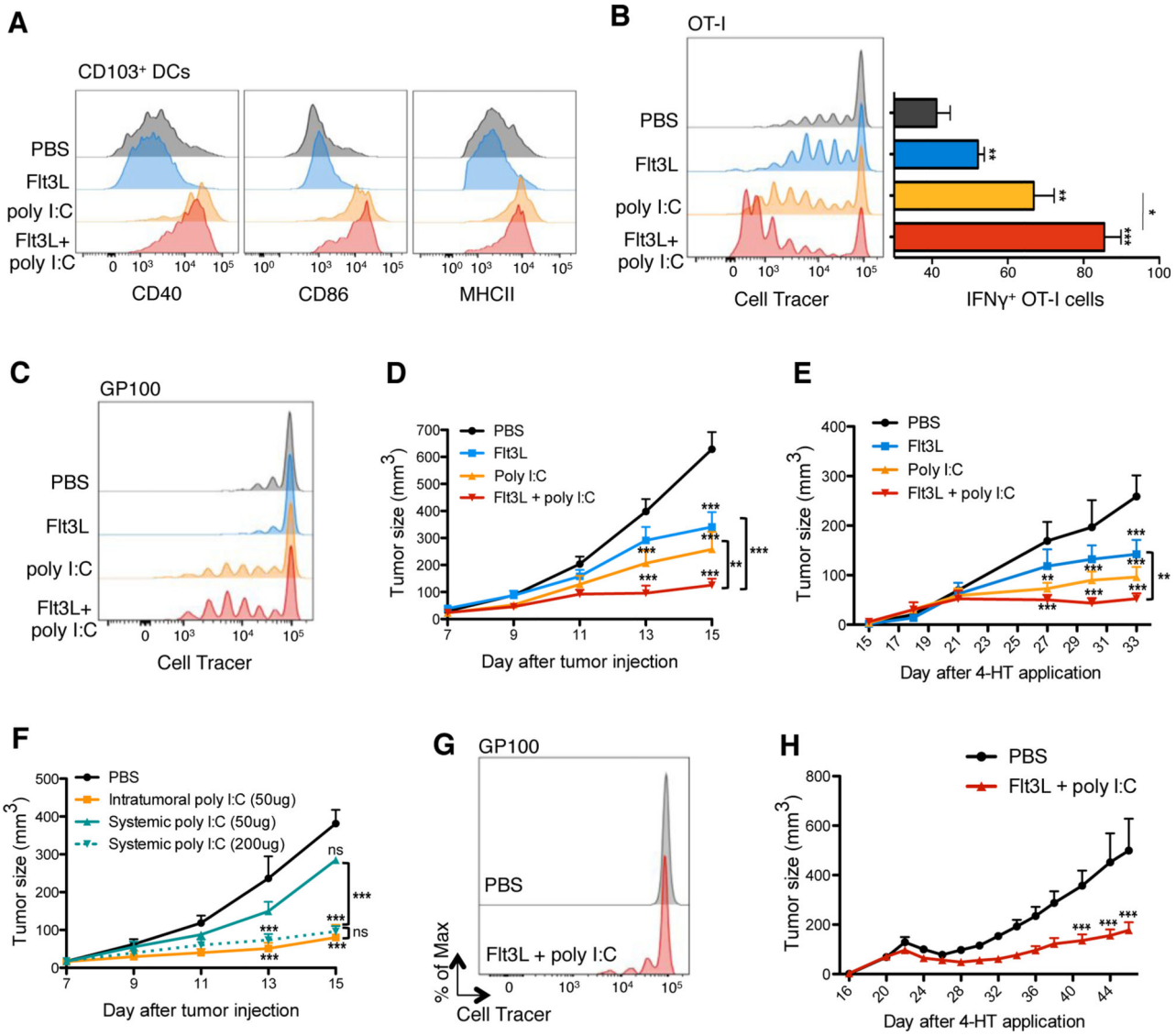

Figure 4. Combination of Flt3L and *in situ* TLR3 ligand promotes the regression of B16 and *Braf*-mutant lesions

(A) Expression of CD40, CD86 and MHCII on tumor-infiltrating CD103$^+$ DCs upon treatment with i.p. FL and/or pIC or PBS as a control (treatment scheme in Figure S4A). Shown are representative histograms of 2 independent experiments.

(B) B16-OVA bearing mice were treated with FL and pIC as in (A). At day 11, mice were adoptively transferred with Violet-labeled OT-I T cells, 2 hrs after the last injection of pIC/PBS. TdLN were harvested 3 days after OT-I T cell transfer and proliferation was assessed based on Violet dilution using flow cytometry. Left panels show a representative histogram showing violet cell dilution in gated transferred OT-I T cell. Bar graph (right panel) shows the mean ± SEM IFNγ production by gated OT-I cells after *in vitro* re-stimulation with ovalbumin$_{257\text{-}264}$ peptide for 4 hrs.

(C) B16-tumors bearing mice were treated with FL and pIC as in (A) and adoptively transferred with Violet-labeled gp100-specific T cells. TdLN were harvested 4 days after i.v. injection of gp100-specific T cells and their proliferation was assessed based on Violet

Author Manuscript Author Manuscript Author Manuscript Author Manuscript

dilution using flow cytometry. Shown is a representative histogram of 2 independent experiments.

(D) B16 tumor-bearing mice were treated with FL, pIC, FL+pIC or PBS as shown in (A). Graph shows the mean tumor growth ± SEM of 4 independent experiments (n=7-12).

(E) *Braf*-mutant tumor bearing mice were treated as in (A), with FL injections starting on day 15 after 4-HT application. Graphs show the mean tumor growth ± SEM of 2 independent experiments (n=5).

(F) B16 tumor-bearing mice were treated with PBS (control) or pIC (50μg or 200μg) intratumorally or i.p.. Graph shows the mean tumor growth ± SEM of 2 independent experiments (n=3-6 mice).

(G) *Braf*-mutant tumor mice were treated as described in Figure S4B. On day 26, 2h after the last injection of pIC/FL/PBS, mice were adoptively transferred with Violet-labeled gp100-specific T cells. TdLN were harvested 4 days after gp100-specific T cell transferred cells and proliferation was assessed through Violet-Cell trace dilution. Shown is a representative histogram of 2 independent experiments.

(H) *Braf*-mutant tumor mice were treated as described in Figure S4B. Graph shows the mean tumor growth ± SEM of 2 independent experiments (n=5-6 mice).

See also Figure S4.

Author Manuscript Author Manuscript Author Manuscript Author Manuscript

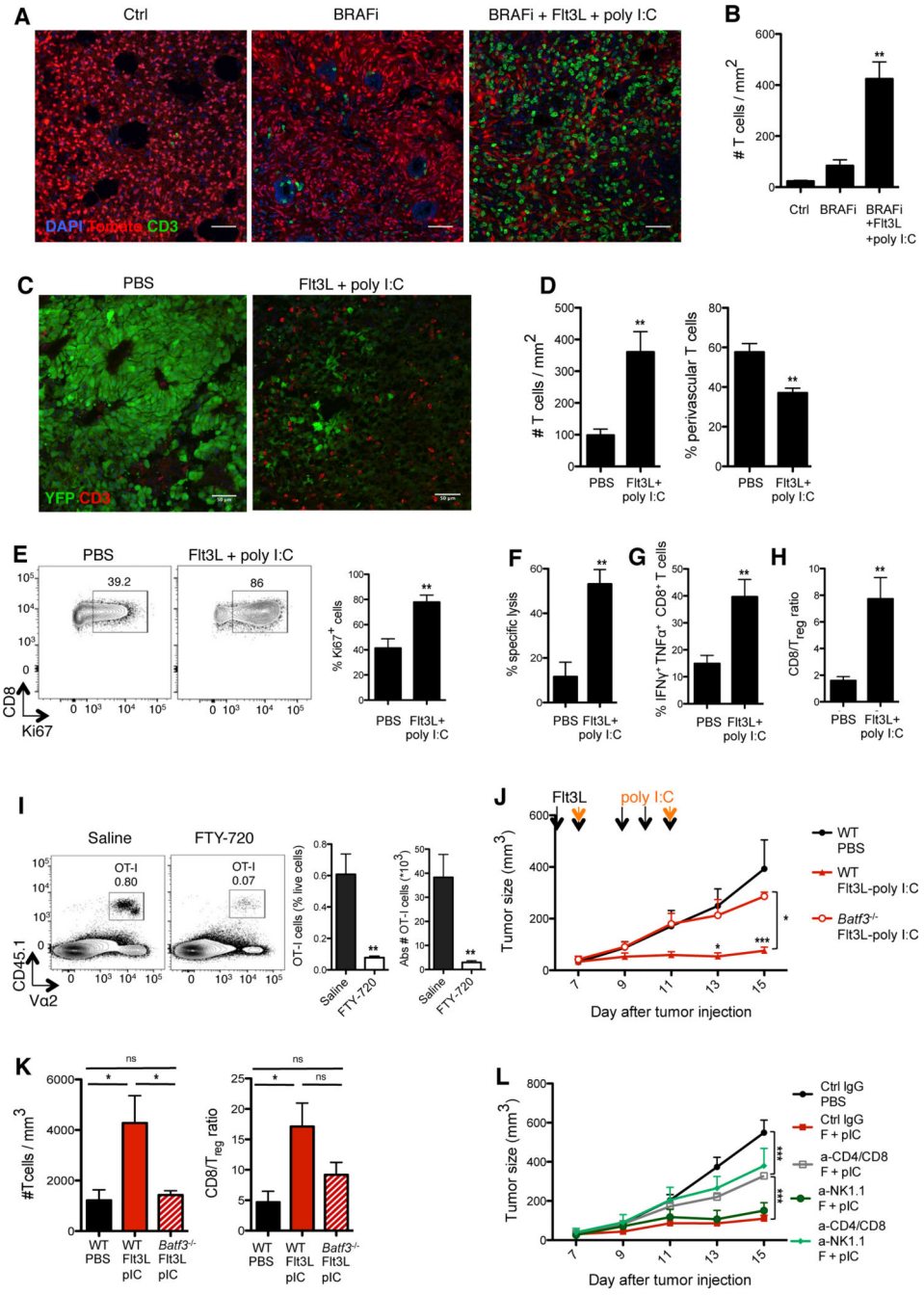

Figure 5. Therapeutic immunity induced by Flt3L-poly I:C combined therapy requires CD103$^+$ DCs and type I IFN

(A-B) Tomato$^+$ *Braf*-mutant tumor mice were treated as described in Figure S4B. Two days after the end of treatment, tumors were harvested and frozen. (A) Representative confocal images of CD3$^+$ T cells (green) infiltrating tumors from the indicated treatment groups. (B) CD3$^+$ T cell density was quantified from confocal images using Cell Profiler software. Shown is the mean ± SEM of 2 independent experiments (n= 3-4;12-16 tiled 20x images were analyzed per animal). (C-D) B16-YFP tumor-bearing mice were treated as described in Figure S4A. Two days after the end of treatment, tumors were harvested and frozen. (C)

Author Manuscript Author Manuscript Author Manuscript Author Manuscript

Shown are representative confocal images of $CD3^+$ T cells (red) infiltrating tumors treated with PBS or FL-pIC. (D) $CD3^+$ T cell density (left) and proportions of perivascular $CD3^+$ T cells (<30um from $CD31^+$ vessels; right) were quantified from confocal images using Cell Profiler software. Shown is the mean ± SEM of 4 independent experiments (n= 4-6; 12-16 tiled 20x images were analyzed per animal).

(E-H) B16 tumor-bearing mice were treated as in Figure S4A and tumor-infiltrating T cells were analyzed at day 15, unless specified otherwise. (E) Representative dot plots (left) and quantification (right) of the frequency of tumor-infiltrating $CD8^+$ T cells expressing the cell cycle protein Ki67. Graph shows the mean ± SEM of 2 independent experiments (n= 4). (F) WT splenocytes were incubated *in vitro* with $ovalbumin_{257-264}$ peptide and labeled with high concentration of CFSE ($CFSE^{hi}$) or incubated with control medium and labeled with low CFSE concentration ($CFSE^{low}$). Same numbers of $CFSE^{hi}$ and $CFSE^{low}$ splenocytes were coinjected into B16 tumor-bearing mice treated with FL+pIC or PBS at day 16 and analyzed 24hrs later. Shown is the mean ± SEM of one experiment (n=4-5). (G) $CD8^+$ T cells were analyzed for IFNγ and TNFα production after PMA/ionomycin stimulation. Shown is the mean ± SEM of 4 independent experiments (n=8). (H) Tumor-infiltrating $CD8^+$ T cell/Treg cell ratio as the mean ± SEM of 4 independent experiments (n=8).

(I) Mice bearing B16-OVA tumors received daily FL injections from day 5 to 9 post- tumor challenge followed by one intratumoral injection of pIC at day 9. Two hours after the pIC injection, tumor-bearing mice were injected with 3×10^6 naïve tumor antigen-specific $CD8^+$ T cells (OT-I) in the presence or absence of the S1P receptor antagonist FTY-720 (from day 9, daily injection as described in the methods). Shown are representative dot plots (left) and quantification of the frequency and absolute numbers of tumor-infiltrating OT-I cells (right) four days after adoptive cell transfer. Graphs show the mean ± SEM of 2 independent experiments (n= 4-5).

(J-K) B16 tumors were injected into WT mice or *Batf3*$^{-/-}$ mice and treated with FL+pIC. Here mice received only 5 injections because $CD103^+$ DCs reappear in *Batf3*$^{-/-}$ mice upon 9 FL injections. (J) Graph shows the mean tumor growth ± SEM of 2 independent experiments (n= 4-6). (K) B16 tumors were harvested on day 15. Bar graphs show the intratumoral T cell density as measured by flow cytometry (left) and $CD8^+$ cell/Treg cell ratio (right) in *Batf3*$^{-/-}$ versus WT treated mice. Results are shown as the mean ± SEM of one experiment (n=4-5).

(L) B16 tumor-bearing mice treated with FL-pIC with with anti-CD4, anti-CD8, anti-NK1.1 Ab or control IgG as described in the method section. Graph shows the mean tumor growth ± SEM of 2 independent experiments (n=3-9).

See also Figure S5.

Author Manuscript Author Manuscript Author Manuscript Author Manuscript

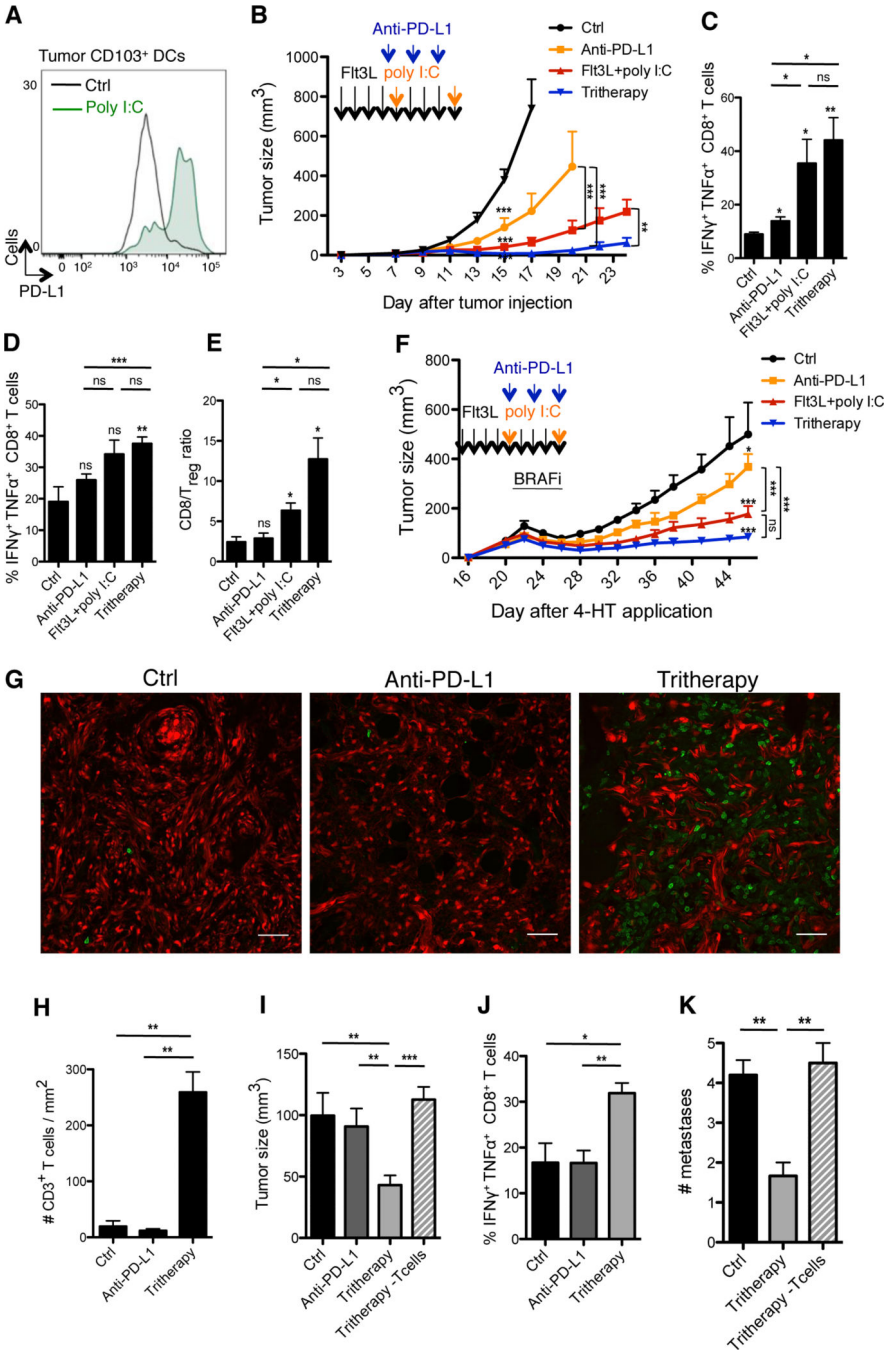

Figure 6. Flt3L and poly I:C synergize with anti-PD-L1 Ab treatment to enhance anti-tumor responses to BRAF inhibition

(A) B16 tumors were injected with 50μg pIC or PBS, on days 7 and 11. Histograms show PD-L1 expression on tumor-infiltrating CD103$^+$ DCs, 2 days after the last pIC or PBS injection with one representative example for each group.

(B) B16 tumor-bearing mice were treated with FL-pIC and injected with anti-PD-L1 mAbs or isotype control on days 7, 9 and 11 and assessed for tumor growth. Graph shows the mean tumor growth ± SEM of 3 independent experiments (n=5-10).

Author Manuscript Author Manuscript Author Manuscript Author Manuscript

(C-E) B16 tumor-bearing mice were treated as in (B). On day 15, mice were sacrificed and $CD8^+$ T cells isolated from the TdLN (C) or tumors (D) were analyzed for the production of IFNγ and TNFα. Shown is the mean ± SEM of 2 independent experiments (n=3-7). (E) Bar graph shows the intratumoral $CD8^+$ cell/Treg cell ratio as the mean ± SEM of 2 independent experiments (n=3-7).

(F) *Braf*-mutant tumor-bearing mice were treated as indicated by the arrows. In addition to FL-pIC±anti-PD-L1 Ab therapy (or PBS and rat IgG as a control), all mice were treated with BRAF inhibitors (BRAFi) admixed chow for 4 days from day 22 to 26. Graph shows the mean tumor growth ± SEM of 2 independent experiments (n= 6-12).

(G-H) $Tomato^+$ *Braf*-mutant tumor bearing mice were treated with the tritherapy, anti-PD-L1 Ab alone or PBS/IgG alone and re-challenged 4 weeks later with 4-HT on the other flank, as described in Figure S6A. (G) Representative confocal images of $CD3^+$ T cells (green) infiltrating the re-challenged tumor. (H) T cell density quantified by histology using Cell Profiler software. Shown is the mean ± SEM of 2 independent experiments (n=3).

(I-J) *Braf*-mutant tumor and TdLN analyses were performed 4 weeks after the tumor re-challenge, as in (G). (I) Volume of the re-challenged tumors. (J) Proportions of $CD8^+$ T in the LN draining the re-challenged tumor producing IFNγ and TNFα after PMA-ionomycin stimulation. Shown is the mean ± SEM of 2 independent experiments (n=5).

(K) Mice were treated as in Figure S6A and the number of skin tumors was assessed a month after the end of treatment. Bar graph shows the mean number of skin tumors ± SEM of 2 independent experiments (n=5-6).

See also Figure S6.